analytical chemistry

pubs.acs.org/ac

Article

Navigate Flying Molecular Elephants Safely to the Ground: Mass-Selective Soft Landing up to the Mega-Dalton Range by Electrospray Controlled Ion-Beam Deposition

Andreas Walz, Karolina Stoiber, Annette Huettig, Hartmut Schlichting,* and Johannes V. Barth*

Cite This: *Anal. Chem.* 2022, 94, 7767−7778

Read Online

ACCESS | Metrics & More | Article Recommendations | Supporting Information

ABSTRACT: The prototype of a highly versatile and efficient preparative mass spectrometry system used for the deposition of molecules in ultrahigh vacuum (UHV) is presented, along with encouraging performance data obtained using four model species that are thermolabile or not sublimable. The test panel comprises two small organic compounds, a small and very large protein, and a large DNA species covering a 4-log mass range up to 1.7 MDa as part of a broad spectrum of analyte species evaluated to date. Three designs of innovative ion guides, a novel digital mass-selective quadrupole (dQMF), and a standard electrospray ionization (ESI) source are combined to an integrated device, abbreviated electrospray controlled ion-beam deposition (ES-CIBD). Full control is achieved by (i) the square-wave-driven radiofrequency (RF) ion guides with steadily tunable frequencies, including a dQMF allowing for investigation, purification, and deposition of a virtually unlimited m/z range, (ii) the adjustable landing energy of ions down to ∼2 eV/z enabling integrity-preserving soft landing, (iii) the deposition in UHV with high ion beam intensity (up to 3 nA) limiting contaminations and deposition time, and (iv) direct coverage control via the deposited charge. The maximum resolution of R = 650 and overall efficiency up to T_{total} = 4.4% calculated from the solution to UHV deposition are advantageous, whereby the latter can be further enhanced by optimizing ionization performance. In the setup presented, a scanning tunneling microscope (STM) is attached for in situ UHV investigations of deposited species, demonstrating a selective, structure-preserving process and atomically clean layers.

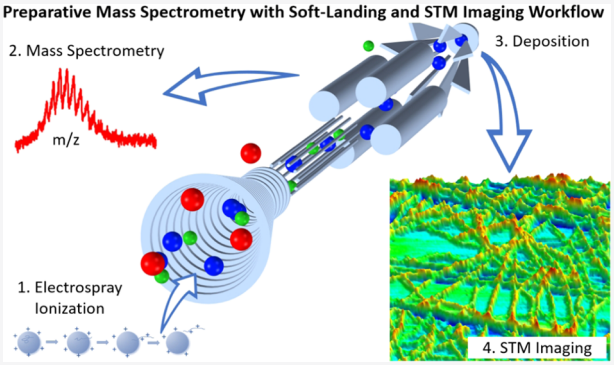

Ion beams with hyperthermal kinetic energies belong to the most versatile tools in chemistry, life science, nanotechnology, and surface science. In the analytical field, they are the basis of commercial mass spectrometers. The ions typically originate from an electrospray ionization (ESI) source, a cluster source, matrix-assisted laser desorption ionization (MALDI),[1,2] or from molecules gathered from a surface under ambient conditions by desorption ESI (DESI)[3,4] or direct analysis in real time (DART)[2,5]—even directly from the tissue of living organisms. The ions are guided through differentially pumped vacuum stages and analytical devices; finally, they are detected while discarded irreversibly. Complementary to these analytical applications, high flux ion beams serve preparative purposes on a deposition target. Beam energies below 10 eV/z are employed for soft landing, i.e., a gentle coating of sample targets, thereby functionalizing these.[6−9] Above 10 eV/z, reactive landing of molecules or clusters prevail, whereas energies substantially above 100 eV/z lead to implantation of atoms or are used for lithographic purposes.[10−12]

Deponents and Integrity. Starting 1977, Cooks pioneered soft landing and reactive landing of mass-selected small ions using a home-built machine that runs at deposition energies as low as 10 eV/z and beam currents up to 10 nA under ultrahigh vacuum (UHV), generated in an electron impact source.[13−15] Hereafter, soft landing has been defined as the deposition of intact species of proper integrity.[16] In 1999, soft-landed DNA was recovered from a membrane, and its functionality was proven by subsequent analysis via polymerase chain reaction (PCR).[17]

Cooks trailblazing experiments in 1977 opened up new pathways toward preparative approaches, though most organic molecules may not be ionized by electron impact. However, ESI sources offering soft ionization suffer from low beam intensities and low overall efficiencies. Thus, several scientific groups stepwise improved their home-built deposition systems aiming for purification and selection of organic substances and the

Received: October 16, 2021
Accepted: March 25, 2022
Published: May 24, 2022

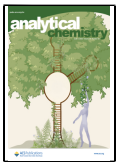

https://doi.org/10.1021/acs.analchem.1c04495
Anal. Chem. 2022, 94, 7767−7778

manufacturing and commercialization of functionalized materials.

Soft and reactive landing under controlled variable kinetic energies—reviewed by Cooks[18]—became the focus of Laskin's[7,19−26] and other groups.[27,28] The technology was applied for the investigation of molecular magnets,[29] organometallic complexes,[24,30−32] the redox activity on surfaces,[33] and chiral features.[34] The possibility to generate chemical gradients on poly(methyl methacrylate) (PMMA) films[35] was demonstrated, and self-assembled monolayers (SAMs) were examined by Cooks and co-workers.[15,16,36,37]

Strong scientific interest in clusters,[38−44] such as the catalytical activity of nanoclusters prepared by ion beams,[24,45−48] and in carbon-based materials, such as graphene,[49,50] carbon nanotubes,[51] and carbon nanoribbons,[52,53] drives activities apart from ESI-based techniques.

The tremendous success of analytical mass spectroscopy focusing on (bio)organic species (metabolites, peptides, proteins, and its complexes) pushed the attention to preparative aspects of these molecules as well. Protein arrays became of strong industry interest,[54−57] but their fabrication is driven by economic aspects.[58] Though proof of concept for preparative soft landing of mass-selected, purified proteins or peptides[41,59−61] as well as a reactive landing for covalent immobilization of biomolecules[22,62] was demonstrated, the low intensity of the ion beam probably blocked maturation to a commercial level. At present, the conformation of biologically relevant molecules on surfaces comes into scientific focus.[61,63−67]

Instrumental Evolution. Compared to Cooks' first experiments,[13] the instrument-based progress achieved to date is significant. Nearly none of the original components survived; however, their functionality was adopted by other elements, seeking to raise beam intensity and quality, throughput, resolution and purity, or reducing complexity.

Cooks' first machine operated electrostatic lenses to focus ions. Radiofrequency (RF) quadrupoles, a complementary principle, were introduced around 1953 by Paul et al.,[68−71] initially for use as mass separators only. These rod-based multipoles use RF voltages of opposite polarity at neighboring electrodes to form a confining potential for ions. Nowadays, both rod arrangements and electrostatic lenses[13,41] are used in the low-pressure regime, where the mean free path of the ions exceeds the (lateral) dimensions of the guide (see Section S2.6, Supporting Information (SI)). Four rods, or rarely up to eight, are common for linear ion guides. Ion traps are equipped with up to 22 rods.[72−76] The dimensions and shape of these rod systems are investigated closely, mainly in their function as mass-selective ion guides.[77−96] The high-pressure regime however is supplied by plate-based or stacked-ring ion guides, colloquial called funnels. The group around Smith[97−103] evolved this concept based on an idea of Gerlich.[84,104−107]

O'Shea's group removed all electrostatic lenses, ion guides, and mass-selective components and simplified the design by skimmers.[108−110] A similar approach directly injects the liquid, thus omitting an ESI source ("pulse injection" or "spray jet technique").[111−114] These loan designs suffer from the lacking mass selection, which results in poor cleanliness and high impact energy of the frozen solvent. Turecek's group made a tradeoff between simplicity and beam quality by combining a funnel with an octupole.[115−117] The reduction of building blocks by a rotating field was proposed[118] and realized later.[119−121] Direct ESI spraying into subambient pressure reduces pumping effort and enhances ionization efficiency.[108,122−126] Micro-electromechanical system (MEMS)-based ion guides for lossless ion manipulation[127−129] enable smaller and more versatile deposition devices.

Though beam quality, operability, and source universality were improved, it had only little effect on the beam intensity. Multiple needles[130−132] and simultaneous deposition of molecules with different m/z under magnetic support[133,134] were proposed and tested to raise beam intensity and throughput. Improvement of the vacuum interface by introducing an inlet-shaped aerodynamic transfer capillary considerably promoted both beam intensity and ion transmission.[135−137]

Additionally, chemical noise and sediments in the ion path were reduced by implementing a jet disrupter in the funnel design.[101,138,139] Removal of unwanted neutrals is also achieved by altered beam geometry: folding[140] or bending beams orthogonally in a transverse quadrupole[19,23,43,141−147] or by curved ion guides.[148−150] The latest approach is the orthogonal arrangement of the transfer capillary relative to the ion funnel.[43,147,151,152] Additionally, this allows for multiple and multiplexed spray systems in parallel.[150,153]

In 1977, Cooks used a Wien filter[13] for mass selection in his first deposition experiments. However, its magnetic field demands high currents, difficult to handle especially under UHV conditions. In contrast, the quadrupole mass spectrometer commonly referred to as a quadrupole mass filter (QMF), first reported by Paul in 1953,[68−71] operates with electrical fields only. Thus, the QMF outperformed the Wien filter in most analytic and preparative applications, though it is not easy to enhance its resolution. Ion traps, implemented in a time of flight (TOF) MS,[154] Fourier transform ion cyclotron resonance (FT-ICR) MS[155] Orbitraps,[156−158] or orbital frequency analyzer (OFA)[159,160] are powerful strategies to increase resolution. They became dominant in analytical MS. However, traps are ineligible for preparative MS, since any type of trap delivers poor, discontinuous beam intensity and prohibits postanalytical usage of the ions. The QMFs currently used in preparative designs[13,133,148,161] report resolutions up to 100 with the reasonable transmission. The early idea from 1973 operating a standard QMF by square waves instead of sinusoidal voltages[162−164] is revitalized due to the progresses in semiconductor technology. However, the actual devices of the group around Reilly, allowing for higher resolutions, are designed for analytic purposes.[165−168] Moreover, mass analyzers allowing for higher intensities come into focus,[118−121] though they currently have poor resolution.

Taking the highly promising concept of preparative mass spectrometry up, we performed a substantial re-engineering: we introduce three innovative ion guide designs, optimized toward high transmission, high flux, and low residual gas load. A novel digital mass filter (dQMF) operating in an unusual square-wave signal mode provides a virtually unlimited mass range of the analyte species. Both in combination with a classical operating ESI source embodies a new, versatile tool for atomic clean nanopreparations as needed in modern surface science. The integrated system, abbreviated ES-CIBD ("electrospray controlled ion beam deposition"), allows for full control of mass, energy, and quantity of the ions. Experiments on several test objects recruited from a broad range of chemical classes demonstrate the high versatility and performance of the system. Based on these data, overall potential of the device is assessed and compared to state of the art.

https://doi.org/10.1021/acs.analchem.1c04495
Anal. Chem. 2022, 94, 7767−7778

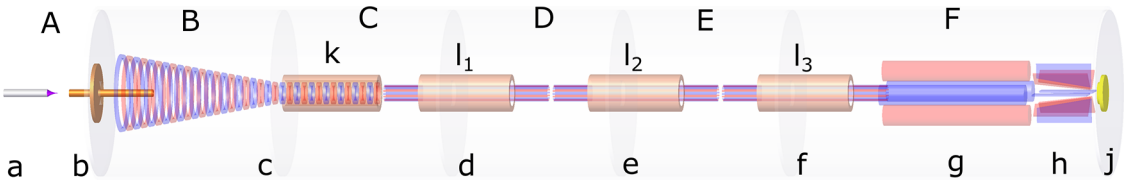

	ambient stage A	vacuum chamber B	vacuum chamber C	vacuum chamber D	vacuum chamber E	vacuum chamber F
pressure [mbar]	1000	2	10^{-2}	10^{-7}	10^{-10}	< 10^{-10}
interfaces	ESI →	capillary	TWIN	SWIG1	SWIG2	SWIG3	dQMF	BLADE	→Target
inscribed diameter [mm]		1.1	30 to 1.5	1.6	2	2.5	16.6	7 to 4	

Figure 1. Overview and key parameters of the ES-CIBD system: (A) electrospray under ambient conditions. (B−F) Subsequent, differentially pumped vacuum chambers. (a) Electrospray emitter at high voltage. (b) Capillary with a funnel-shaped inlet acting as a counter electrode and vacuum interface. (c) Combined funnel and tunnel, forming the TWIN ion guide with strongly reduced gas load. (d−f) Small wire ion guides (SWIGs) with strongly reduced gas load. (g) Digital quadrupole mass filter (dQMF) with virtually unlimited m/z range. (h) BLADE ion guide to refocus the beam. (j) Target on which ions are soft landed. (k,l) Gas-load reduction tubes. Operation pressure and clear diameters of the respective ion guides are summarized in the table. Refer to details in the SI.

EXPERIMENTAL SECTION

A short overview of the ES-CIBD system in its actual realization is shown in Figure 1: an ESI source operating at ambient pressure (A) produces ions from the liquid provided in the emitter (a). The ions are transferred through a funnel-shaped[135] capillary (b) into the first vacuum chamber (B). The subsequent differential pumping chambers (B−F) separate the ions from the unwanted neutrals on their way to the deposition target (j) in UHV. They are guided along their path by an RF ion funnel combined with an ion tunnel (TWIN) (c) and three small wire ion guides (SWIGs) (d−f). A dQMF (g) operates as a mass selector. The focusing BLADE ion guide (h) leads the ions to the sample target (j).

ESI Ion Source. In the setup presented a home-built conventional ESI source without sheath gas assistance (only occasionally operated in an ambient CO_2 environment) is attached to the CIBD system. The emitter (a) is cut from uncoated fused silica tubes with an inner diameter of 50 or 75 μm. It opens into a heated capillary (b) acting as a counter electrode and interface to transmit the ions from the spraying plume into the first vacuum chamber (B). The design of the capillary is adapted from Rauschenbach.[135] It consists of a funnel-shaped inlet followed by a 6 cm long tube with a clear diameter of 1.1 mm.

TWIN Ion Guide. The gas-phase ions leaving the capillary (b) are confined and focused by a novel TWIN ion guide (c). It consists of a standard ion funnel section for focusing,[84,97] located in the first chamber (B), and a tubular sealed ion tunnel section extending into the subsequent chamber (C). Ring electrodes made from metal sheets with 0.2 mm thickness and 0.2 mm spacing keep the ions in path. This elongated pressure interface significantly reduces the gas load compared to a typical thin orifice[84,139,169,170] by a factor of about 20 (see Section S3.5, SI) while preserving the confining properties of the RF field. Another important feature of the TWIN is the applied variable square-wave RF frequency, steadily adjustable from kilohertz to a few megahertz and separately provided to funnel and tunnel region. The optimum in the amplitude/frequency space is chosen, to match the m/z ratio of a guided ion of interest, for maximum transmission. This feature pertains to all other ion guides as well.

SWIG Ion Guide. The novel SWIG (d−f) is a high-order multipole made from tensioned superthin wire electrodes. The advantage of this device is its small total diameter and the strongly reduced profile of the electrodes. Thereby and due to the tube surrounding the wires (l), the gas load between the stages is reduced by a factor of 10 (see Section S3.6, SI) while the RF field is steadily kept. The smallest SWIG adopted consists of 16 wire electrodes of 0.18 mm diameter aligned in parallel and uniformly distributed on a circle around a central axis with a clear diameter of 1.6 mm, defining the very upper diameter of the ion beam. The high number of electrodes generates a short-range high-order multipole field with steep effective potential walls for a nearly lossless transfer of ions and an almost field-free center region.[84] This field-free area allows for injection and transfer of ion beams with a size close to the clear diameter. A further advantage of the small distance between the electrodes is the low RF voltage needed, as the enclosing potential of an RF guide depends upon the electric field, whereas the RF heating of the ions depends upon the voltage. Thus, the RF heating of the ions is opposite to the size of the electrode structure; see Section S3.2, SI.

dQMF Mass Filter. A common 19 mm quadrupole rod system from Extrel with pre- and postfilters is operated with home-built electronics. Unlike every commercial QMF known to us, it does not operate with a resonantly generated sine-shaped voltage but in a "digital" mode. The RF signal is a computer-controlled square wave with steadily variable frequency and amplitude. Due to the tunable frequency, which is adapted to the mass of the molecules under investigation, the optimum RF parameters for each molecule can be chosen. There is virtually no limit for the accessible m/z range of the transmitted molecules (see Sections S3.1 and 4, SI). To our knowledge, this flexibility is currently not achieved by any other QMF. The dQMF accomplishes both tasks of the CIBD system—the analysis of the ion beam and the selection of distinct species during deposition.

BLADE Ion Guide. A BLADE (h) consists of 16 radially arranged metal sheet electrodes, which approximate a conical high-order multipole. The electrode sheets have a thickness of 0.5 mm and focus the ions from 7 mm diameter at the inlet to 4 mm at the outlet, adapted to the sample diameter.

Further details of the components are provided in the SI.

https://doi.org/10.1021/acs.analchem.1c04495
Anal. Chem. 2022, 94, 7767−7778

RESULTS AND DISCUSSION

The described new CIBD soft landing system was tested by means of a standard ESI source and a scanning tunneling microscope (STM) to demonstrate its flexibility. The sprayed molecules were chosen in accordance with the parameters to be tested. Surface data presented refer to ions soft landed on Ag(111) or Cu(111) single crystals for further investigation by a variable temperature STM in UHV.

Resolving Isotopologues of Rhodamine B (RhoB). The frequently used test molecule rhodamine B[171−178] was sprayed in a positive mode generating an ion beam dominated by the single-charged cation (Figure 2). The overview spectrum and the inset give a first idea of the tradeoff between high selectivity for clean depositions and high transmission for fast depositions. For the overview spectrum, a resolution of about $R = \frac{m/z}{\Delta m/z} = 110$ (full width at half-maximum, FWHM) was chosen. Few minor intensity peaks are found at slightly lower m/z, but only one very dominant charge state of the rhodamine B cation is present at 443 Th. The inset of Figure 2 presents a series of spectra with increasing resolution up to $R = 670$, revealing a second peak of the rhodamine B cation, approximately one mass apart from the main peak. Both isotopologues are generated by a replacement of C12/C13 in the molecule at a single, arbitrary position. The natural abundance of C^{13} of about 1% translates into a prevalence of 28% in the rhodamine B isotopologues with 28 potential C positions.[2,179,180] This value is experimentally confirmed by the relative height of the C^{13}-containing peak versus the "main" peak with 100% C^{12} content (Figure 2). Notably, unlike many other deposition instruments,[41,53,148,181,182] beam characterization and deposition are performed with the same m/z-selective device. Though the resolution is lower, e.g., compared to a TOF,[41] our design works as "what you see is what you get" on the sample.

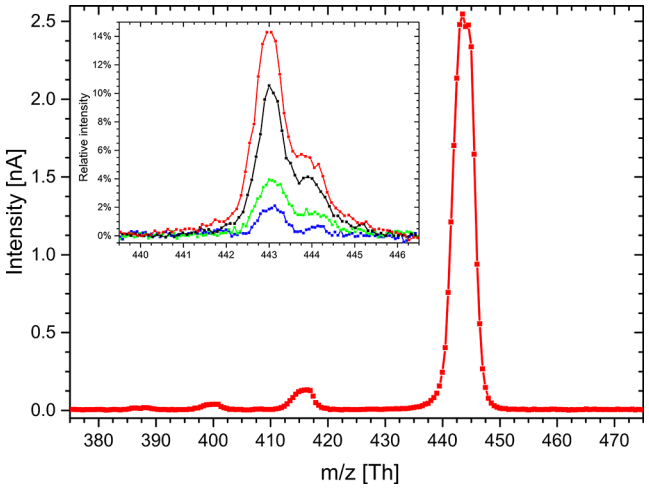

Figure 2. High-intensity mass spectrum of rhodamine B with a resolution $R = 110$ (FWHM) dominated by the single-charged cation. Inset: Spectra from resolution assessment with $R = 530$ (red) to $R = 670$ (blue); $m/z = 443$ Da for the all-C^{12} isotopologues; and $m/z = 444$ Da for species with a single C^{13}. Transmission scale in the inset is normalized to 100% at $R = 55$.

The advantage of rhodamine B as a test molecule is its very decent spray behavior due to its high solubility and its ionic nature, as well as its high stability and availability. According to the mass spectrum, the ion beam almost exclusively consists of one ion species. Thus, rhodamine B qualifies as an ideal model system to analyze system parameters (Figures 2 and 6). The efficiency of an ion ejected by the ESI source, mass filtered and soft landed on the sample surface (transmission efficiency), can be estimated to about 22% at $R = 110$ (Table 1).

Charge States, Conformation, and Adducts of Insulin. Insulin serves as a test object exemplary for the group of nonelongated biomolecules. The globular 5.8 kDa[183−185] protein adopts several charge states in addition to the metabolic active monomeric form which dominates at physiological conditions in serum.[186] Dependent on the solvent conditions, insulin builds various nonactive oligomeric stages in vitro: low ionic strength, low pH, and low concentration of the protein promote rather monomeric and dimeric states, while higher pH, higher concentration, high ionic strength, divalent metal ions, chloride, and phenolic compounds drive assembly to tetramers, hexamers, or even higher structures including aggregates.[185,187−195]

Due to the virtually salt-free spray conditions and low protein concentrations at acidic pH, primarily monomers, potentially

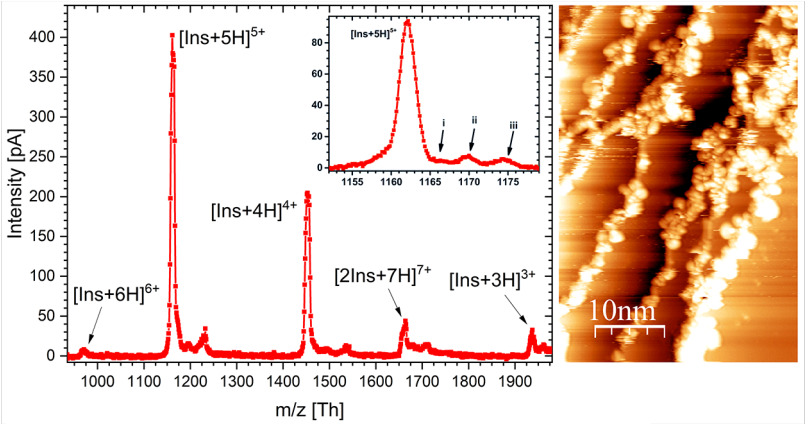

Figure 3. Left: Mass spectrum of insulin ($R = 130$) showing two prominent monomer signals (4+ and 5+ charged), two lower intensity monomer peaks (6+ and 3+), and an odd protonated dimer (7+). Inset ($R = 490$): Three emerging satellite peaks are attributed to adducts with (i) sodium [Ins + Na + 4H]$^{5+}$, (ii) potassium [Ins + K + 4H]$^{5+}$, and (iii) acetic acid [Ins + AcAc + 5H]$^{5+}$ or [Ins + K + Na + 3H]$^{5+}$ (see the SI). Right: Postdeposition STM image on Cu(111). Insulin monomers and dimers of various charge states preferably decorate step edges including building of large clusters after landing.

https://doi.org/10.1021/acs.analchem.1c04495
Anal. Chem. 2022, 94, 7767−7778

accompanied by low yields of dimers, are expected in our experiments. According to sequence, insulin in the solution can be protonated at its four basic amino acids and N-termini of its two subunits. In ESI processes, however, protein and droplet surface area, affected by flow rate and diameter of the emitter, play a dominant role in charging efficiency.[196,197] Conducting Rayleigh limit calculations[198] of a sphere at standard conditions, a monomer should carry six and a dimer eight charges at maximum, confirmed by experimental data,[187] while monomers with eight charges are observed using supercharging agents.[199]

The ES-CIBD delivered results as expected: the overview spectrum is dominated by two main peaks representing the 4+ and 5+ charged monomers in addition to less abundant peaks of monomeric molecules with 3+ and 6+ charges according to mass calculation (Figure 3). In principle, some of these peaks may be overlaid or even replaced by the respective double-charged dimers (e.g., $[Ins + 3H]^{3+}$ by $[2Ins + 6H]^{6+}$), while those cannot be distinguished by m/z measurements. Additional low abundant peaks may be attributed to either dimers or adducts. Hints for dimers are given by a peak compatible with the odd charged oligomeric form $[2Ins + 7H]^{7+}$. This peak is consistent with a similar peak identified by the Robinson group as a dimer species with seven charges.[187] For the insulin concentration tested, the respective dimers are quite likely to coexist as those emerge at levels as low as 2% of the concentration we used. The probability of dimers strongly increases with rising concentrations.[187] Hexamers or even higher oligomeric states seem less likely, as the electrolyte composition favors smaller entities (Figure 3).

Generation of adducts with monovalent metal cations (sodium, potassium) by ESI is known to intensify with increasing emitter sizes and flow rates and adversely affects resolution.[200] This is also reported for insulin.[197,201] Additionally, water adducts are described for insulin hexamers.[202] Possibly those adducts might emerge with our setting too, as suggested by the details in the inset of Figure 3. In particular, three low-intensity signals appear in close proximity to the 5+ charged variant. By calculating the calibrated mass, these can be attributed to insulin 5+ monomers carrying single sodium or potassium ions,[203] or a single acetic acid (AcAc) molecule (Figure 3, inset, peaks (i)−(iii) respectively). The likelihood of other adducts is discussed in a mass deviation assessment (SI). Similar observations are made for the 4+ peak (data not shown).

Monomers, dimers, and hexamers are considered native states of insulin. ESI, however, may produce also higher oligomers which, due to their correlation with the insulin concentration, are regarded ESI "artefacts".[204] In such event, aggregates were easily excluded by m/z-filtering during deposition. Putative aggregates that emerge during sample preparation prior to ESI can successfully be removed by spin filtration.[205] In our case, the main peaks observed match with the theoretical masses of commonly charged monomeric and dimeric states. This and the lack of higher oligomers suggest that the ES-CIBD system preserves the states of the molecules provided in the solution.

Charge State Modulation of a Porphyrin Variant. The synthetic copper incorporated 5,10,15,20-tetrakis(4-carboxylphenyl)-porphyrin (Cu-TCPP) with a mass of 854 Da belongs to the group of porphyrins extensively used and investigated due to their biological relevance as a reactive component in hemoglobin, chlorophyll, and other biomolecules, as well as their metal organic nature.[206,207] Forming nanosheets of metal organic frameworks (MOF), Cu-TCPP is prominent in the detection of DNA.[208−210] It is explored by scanning probe microscopy (SPM) in liquid[211] and after classical UHV deposition techniques.[212,213]

We used Cu-TCPP in an electrospray ionization setting. Ionization was achieved by negative spray mode supported by the proton acceptor ammonia. Similar to insulin, multiple charge states are present, with double and triple charged states being predominant in all settings. Higher charge states rise with higher ammonia concentration (Figure 4). Single charge states are

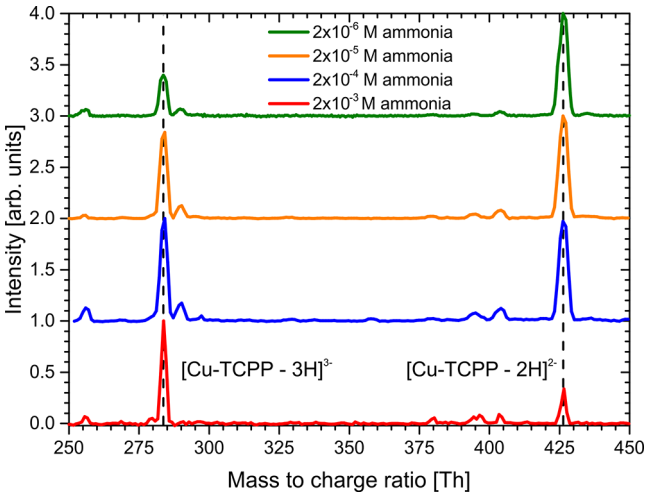

Figure 4. Mass spectrum of Cu-TCPP (8×10^{-5} M) in negative spray mode at varying ammonia concentrations. The values of the two main peaks are 283.7 and 426 Th, respectively. Main peak intensities are normalized to 1, for comparison reasons.

observed as well, however, at low H-acceptor concentrations only. Exemplary, with 2×10^{-4} and 2×10^{-5} M ammonia, intensities of 4 and 15% with respect to the main peak are seen (data not shown). Thus, modulation of charge states by varying acceptor concentrations is feasible.

Our experiments on Cu-TCPP demonstrate one advantage of ESI mass spectrometry regarding preservation and proof of the integrity of the molecules. It is an accepted fact that the structural stability of evaporated organic substances becomes challenging with rising molecule size.[214−216] SPM measurements of larger and three-dimensional molecules become more challenging and all structural features may not be resolved anymore. Preparative mass spectrometry may serve as a method to prove at least the weight of a deposited large organic molecule as a surrogate for its integrity. Mass can be predicted from a suitable precise mass spectrum by analyzing the peak distance of two charge states. In our case, the difference of the back-calculated masses of the double and triple charged species agrees with the expected difference of a proton mass. This relation does not apply to any truncated molecules nor to adducts, confirming Cu-TCPP integrity in our experiment. In contrast, upon organic molecular beam epitaxy (OMBE) deposition, the molecule was found impaired due to a presumed decomposition of the carboxylic groups, deduced from a carbon dioxide peak emerging in the residual gas spectrum upon annealing.[217] This is in accordance with the integrity-preserving nature of ESI demonstrated by other authors performing ESI deposition experiments on fragile molecules such as proteins, oligoynes, dyes, or cluster.[28,29,32,53,59,175,218−220]

Impurities by fragments or residual solvent molecules in the ES-CIBD are negligible due to a stringent m/z selection and the UHV conditions. Even the lack of two or three protons caused

https://doi.org/10.1021/acs.analchem.1c04495
Anal. Chem. 2022, 94, 7767−7778

by the negative electrospray process—in Cu-TCPP presumably at the carboxylic groups—will be restored after landing, since hydrogen as the dominant residual gas is still present in a "clean" UHV environment of 10^{-10} mbar.[221]

Deposition of Large String-like DNA. As a representative molecule for rather large and elongated molecules such as nucleic acids, the double-strand (ds) circular plasmid pUC19 was processed.[222] The bacterial DNA, adopting a B-form helix,[223] consists of 2686 base pairs translating into a molecular mass of approximately 1.7 MDa. Data were obtained by spraying an aqueous solution of pUC19 with 66% acetonitrile (ACN) as an organic component. At these conditions, dsDNA molecules carry negative charges predominantly on the phosphate backbone accessible for electrospray ionization in negative mode.

In the mass spectrum, pUC19 appears as a broad distribution of charge states between 1150 Th and about 2000 Th, which cannot be resolved individually (Figure 5D). This broad curve is

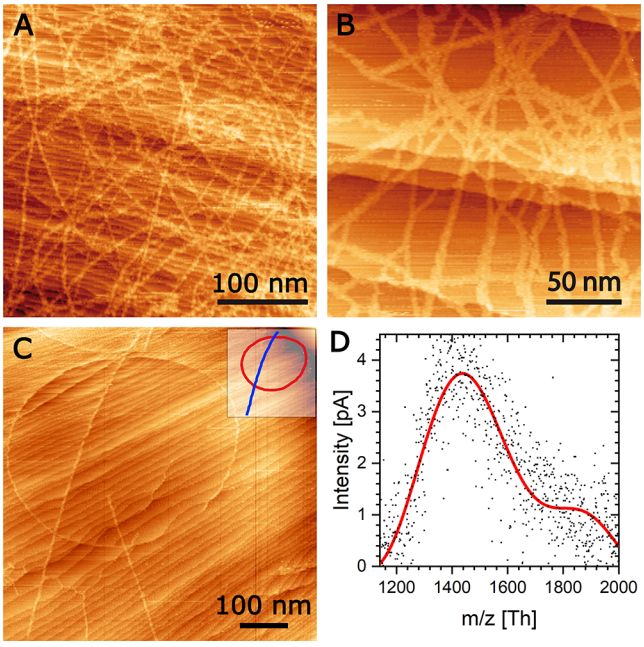

Figure 5. Deposition of plasmid DNA (pUC19, 1.7 MDa mass). (A–C) RT-UHV-STM analysis on Ag(111). (A) High coverage of multiple strands crossing (U = 1.3 V; I = 90 pA). (B) Close-up view with helical twisted and supercoiled strands crossing step edges of the crystal (U = 1.3 V; I = 10 pA). (C) Low coverage with two individual circular plasmids appearing as relaxed ring and supercoiled rod, respectively. Inset: Schematic of (C). (D) Mass spectrum of pUC19. Raw data (dots); guide-to-the-eye (red).

similar to those obtained by others with related plasmid-type species using ESI-MS.[224] The m/z center of gravity around 1500 Th translates into approximately 1100 elementary charges per DNA molecule. This is roughly 10-fold higher than expected for the maximal charging deduced from the Rayleigh limit[198] for a globular molecule in an aqueous solution. This elevated number of charges, which is also experimentally determined by other groups using charge detection mass spectrometry on various DNA molecules,[225,226] indicates that the globular Rayleigh model seems not reasonable for rather elongated molecules. Assuming a cylindrical shape instead, the corresponding cylindrical Rayleigh limit of 1100e (details in the SI) is consistent with the experimental results. The experimental maximum charging per molecule of ~1500 can be deduced from the actual m/z lower boundary (~1160). This value is higher than the Rayleigh limit would predict, suggesting a kind of overcharging. Further, the number of phosphodiester residues assumed to carry the negative charges of DNA in solution (5372 in pUC19) obviously plays a minor part in an ESI environment. For an attempt to interpret the apparent second population (the curve shoulder to the right of the main peak in D), please refer to the SI.

As a general consequence of the elongated appearance, the transition from charged droplets produced by the ESI source to single gas-phase ions very likely follow the chain ejection model (CEM), in contrast to the charge residue model (CRM)[227] applicable for the previous test molecules.

For DNA depositions,[205] the dQMF was operated in an RF-only mode at 1100 Th, i.e., cutting all masses below this threshold and transmitting all charge states attributed to pUC19. After high-density deposition, circular plasmid DNA molecules appear as a quite crowded chaotic mesh, where single molecules are hardly be distinguished (Figure 5A,B). Higher resolved images on Cu(111) allow for a differentiation between helically twisted and supercoiled pUC19 (data not shown). Lower coverages evoke single species (Figure 5C). Here, the accurate geometric shapes are remarkable, in contrast to serpentine appearance at drop casting.[228] This may be caused by the high number of charges on the molecule close to the cylindrical Rayleigh limit obtained during the ESI process, resulting in a high Coulomb repulsion and a balloon shape at the beginning of the landing process[229] before discharging. No impurities are visible aside from the clearly recognizable DNA molecules, which appear intact.[230−233]

ES-CIBD Performance. The requirements for a soft-landing machine deviate from an established analytical mass spectrometer mainly by much higher intensities and also by well-defined low kinetic energies of the ion beam. The m/z range is important to investigate possibly interesting materials. The "total efficiency" of a preparative machine corresponds to the "sensitivity" of an analytical machine: While the high m/z resolution R is compulsive for an analytical machine, this ends up in a tradeoff with the beam intensity as the dominant parameter of a preparative machine. For the ES-CIBD system, the beam intensity even almost entirely depends on the ionization efficiency of the deposited molecules. However, transmission efficiency and saturation in the ion guides are basically constant parameters of our frequency-adapted hardware.

The currents listed in Table 1 depend on the concentration of the specimen in the sprayed solution, certainly among other parameters affecting the spray process. Mean values at the

Table 1. Deposition Parameters

molecule	rhodamine B	Cu-TCPP	insulin	pUC19
molecular weight	443 Da	854 Da	5.8 kDa	1.7 MDa
molarity [M]	10^{-4}	8×10^{-5}	8×10^{-5}	10^{-8}
sample current	+2.2 nA	−0.4 nA[a]	+0.4 nA[a]	−0.4 nA
spray eff. = T_{ESI}	12%	1.4%	3.2%	20%
transmission eff. = T_{CIBD}	22%			
overall efficiency[b] = T_{total}	2.7%	0.30%	0.71%	4.4%

[a]Current for one (main) peak determined when multiple distinct peaks are present; here, $[Cu\text{-}TCCP]^{2-}$, $[Ins]^{5+}$. [b]Overall efficiency including all analyte peaks if multiple are present.

https://doi.org/10.1021/acs.analchem.1c04495
Anal. Chem. 2022, 94, 7767−7778

sample are obtained near the optimum parameters. The typical current at the capillary outlet is 10 nA for rhodamine B.

The amount of specimen transmitted through the CIBD system to the sample is expressed as the overall efficiency[224−226] $T_{Total} = \frac{\text{deposited molecules per s}}{\text{sprayed molecules per s}}$. Other authors used the terms "overall soft-landing yield"[54,128,142,227] or "total efficiency".[141] T_{Total} cannot be measured directly, the number and charge of molecules possibly generated by ESI, has to be known. This "utilization efficiency" depends strongly on the sprayed molecule[234] and the construction of the ESI source.[135,137] We refer to it as $T_{ESI} = \frac{\text{current leaving capillary}}{\text{charge of sprayed molecules per s}}$. Combined with the transmission efficiency of the CIBD system downstream of the capillary, $T_{CIBD} = \frac{\text{current at sample}}{\text{current leaving capillary}}$, the overall efficiency is $T_{Total} = T_{ESI} \cdot T_{CIBD}$. Overall efficiencies are listed in Table 1 (see details in the SI).

For comparison, in 1977, Cooks[13] achieved a deposition current of 10 nA, mass selected with $R = 100$. Though he used an electron impact source, this early experiment is remarkable, as it demonstrates that the ion generation and the primary transfer into vacuum are limiting, not the capacities downstream. Mass-selected ESI spray started[41,59,63,133,135,145−148,235] in the 21th century. The Laskin group reports up to −4.6 nA for negative spray and 8.2 nA for positive spray, respectively, in the same device.[150]

According to literature, mass-selected overall efficiency T_{Total} ranges from 10^{-5} to 1.6%.[59,60,133−135,137,147−150,236−239] Note the prevailing influence of the molecule as well as the different resolutions of the mass-selective devices, as listed in the SI. Furthermore, the diameter of the ESI emitter from 100 μm down to 1 μm (nanospray) has substantial relevance to the overall efficiency. With decreasing droplet size (by use of smaller emitters), T_{Total} increases. Assuming an optimized specimen concentration, the probability for a droplet containing no or multiple specimen molecules is reduced.

There is a tradeoff between resolution and transmission in any mass spectrometer. Moreover, the number of oscillations of an ion in the RF field is crucial. Basically, our design allows keeping the number of oscillations of an ion constant during an m/z scan. This is achieved by adapting the frequency versus kinetic energy (see Section S3.8, SI). However, this feature needs further enhancement of the software. Transmission T_{dQMF} as a function of resolution R is shown for rhodamine B and insulin for analysis as well as for deposition (cf. Figure 6).

Soft landing and reactive landing demand a defined kinetic energy of molecules to be deposited, i.e., energy broadening is relevant. The mean landing energy may be changed via the sample potential versus kinetic energy of the ions, which is defined in chamber C. Downstream, ion mean free path is too long. The deposition current as a function of the sample potential was exemplary recorded using Cu-TCPP (Figure 7). The first derivative gives an energy broadening of about 2.2 V at FWHM. Thus, molecules with kinetic energies below 2 eV/z may be deposited with reasonable intensity, well below the soft-landing limit of about 10 eV/z.

Finally, the measurement of the deposition current over time provides access to the amount of deposited charge, i.e., the number of landed molecules can be calculated through the charge state known from MS.

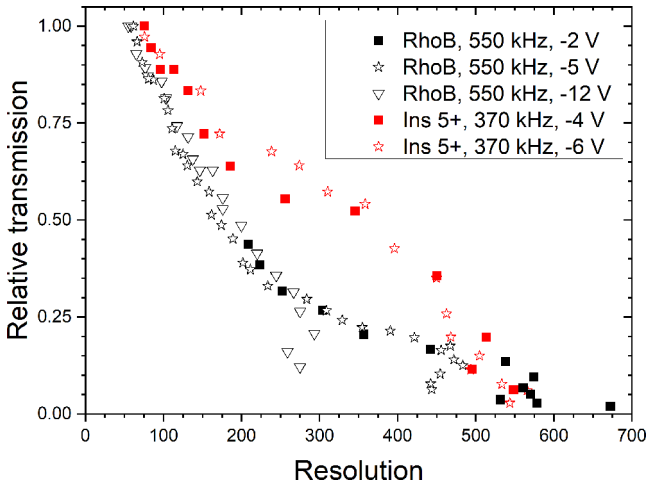

Figure 6. Resolution vs peak transmission of the dQMF. Data points are normalized with their corresponding highest transmission value. Test ions are the rhodamine B cation and the insulin 5+ ion (see Figures 2 and 3). Operation frequencies of the dQMF and field axis potentials with respect to chamber C are given in the legend.

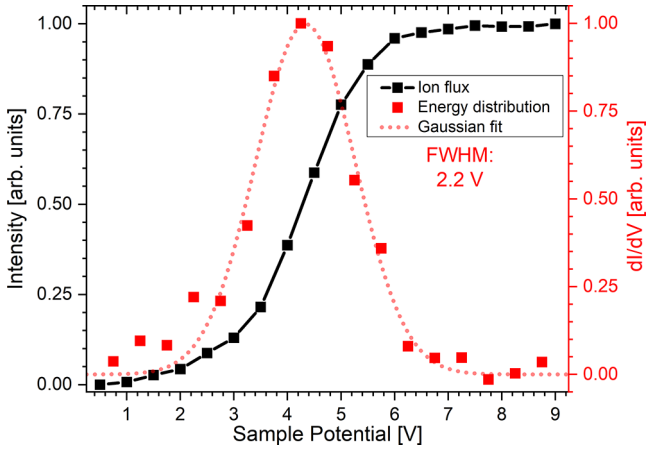

Figure 7. Kinetic energy of Cu-TCPP molecules measured via ion flux as a function of sample potential. The derivative of the flux gives the energy distribution of the ions.

SUMMARY AND OUTLOOK

A versatile and efficient CIBD system coupled to an ESI source is presented. It is proven as a valuable tool to make a lot of species "fly": small or simple organic molecules like the porphyrin derivative Cu-TCPP, the larger biomolecules insulin and plasmid DNA with a mass of 1.7 MDa have been soft landed, so as other molecules such as spermine,[205] ZnPC (data not shown), apoferritin (m/z of ~10.000 Th, see Section 4, SI), and nanocarbons like graphene nanoribbons,[240] with no limits in sight.

In the components of this design, several innovative ideas were consequently implemented: (A) tubes instead of standard aperture plates with a diameter as low as possible were inserted to connect two pressure stages. Thereby, the residual gas load was greatly reduced. Coincidently, the transmission efficiency through the tubes is even enhanced, as the guiding RF electrodes were continuously linked between the stages. There is no discontinuity like with an aperture plate. In the high-pressure regime, this concept was realized by combining an ion funnel with an ion tunnel to form a TWIN ion guide, resulting in a

https://doi.org/10.1021/acs.analchem.1c04495
Anal. Chem. 2022, 94, 7767−7778

reduction of gas load by a factor of 20 compared to an aperture of the same diameter. In the low-pressure regime, 16-pole wire ion guides with tiny clear diameters (SWIGs) are used, reducing gas load by a factor of 10. (B) Low-amplitude square-wave RF signals, applied to all types of ion guides with steadily variable frequency, allow for a transmission efficiency of typically 80% per ion guide for molecules of any m/z in both pressure regimes. (C) The mass-selective dQMF device is operated with square-wave RF signals as well. As in the ion guides, the steadily variable frequency results in a virtually unlimited m/z range of the investigated and deposited molecules. The transmission at a given resolution is almost independent of the m/z value of a molecule. A resolution up to 150 provides high transmission efficiencies >75%. Reasonable precise selection with a resolution of above 500 still provides 10−15% transmission. The tiny beam diameter of the injecting SWIG combined with the small radial beam energy results in a high injection probability into the dQMF translating into a high overall transmission of the whole CIBD system.

The chosen design results in:

(1) A low energy distribution of about 2 eV/z (Figure 7) allowing for soft landing.
(2) A high deposition current up to 2.2 nA (Table 1).
(3) A transmission efficiency of about 22% over a virtually unlimited range of m/z (see Section S4, SI) combined with a mass resolution up to R = 650 (Figure 6).
(4) A high overall efficiency up to 4.4% (Table 1).
(5) A high degree of system compactness and pumping efficiency combined with a low background pressure below 10^{-10} mbar and high cleanliness (Figure 1).

We want to emphasize that possibly cruising neutrals along the line of sight to the sample, which is often discussed, can be excluded from the STM images and from the tiny diameter of the guides. This design implicitly prevents a straight line of sight.

To our best knowledge, resolution, overall efficiency, and mass range are above values reported for deposition systems in literature (see discussion in the SI).

The described CIBD design reflects the pilot development stage. Clear diameters of the ion guides, their tunnel length, and operating pressure will be optimized further. From the current point of view, at least chamber E might be omitted without deteriorating the pressure level in sample chamber F (Figure 1). Attaching alternate beam sources like a cluster source will unlock further applications.

■ ASSOCIATED CONTENT

Supporting Information

The Supporting Information is available free of charge at https://pubs.acs.org/doi/10.1021/acs.analchem.1c04495.

TOC: Instrumental settings and parameters (Section 1−3, Fig. S1, S2); extension of m/z range (Section 4, Fig. S3); calculation of insulin adducts (Section 5, Fig. S4); calculation of cylindrical Rayleigh limit and DNA MS interpretation (Section 6−7, Fig. S5); overall efficiency benchmarking (Section 8, Fig. S6); typical CIBD parameters RhoB (section 6); experimental details and references (Section 9−10, tables) (PDF)

■ AUTHOR INFORMATION

Corresponding Authors

Hartmut Schlichting − *Physics Department E20, Technical University of Munich, 85748 Garching, Germany;* orcid.org/0000-0001-6421-5076; Email: hartmut.schlichting@tum.de

Johannes V. Barth − *Physics Department E20, Technical University of Munich, 85748 Garching, Germany;* orcid.org/0000-0002-6270-2150; Email: jvb@tum.de

Authors

Andreas Walz − *Physics Department E20, Technical University of Munich, 85748 Garching, Germany*

Karolina Stoiber − *Physics Department E20, Technical University of Munich, 85748 Garching, Germany*

Annette Huettig − *Physics Department E20, Technical University of Munich, 85748 Garching, Germany*

Complete contact information is available at: https://pubs.acs.org/10.1021/acs.analchem.1c04495

Notes

The authors declare no competing financial interest.

■ ACKNOWLEDGMENTS

This work was supported by the ERC Advanced Grant MolArt #247299, the ERC-PoC Grant Softbeam #780907, the FET Innovation Launchpad Grant MolShuttle #946223, and the FET-Open Grant 2D Ink # 664878. The team is supported by the e-conversion excellence cluster of DFG #EXC2089. In the one-decade-long ES-CIBD development history, a number of bachelor, master, and Ph.D. students contributed to this success, mainly: Tobias Kaposi, Michael Walz, Sabrina Sterzl, Theresa Buberl, Nicolo Sernicola, and David Reinisch. The authors gratefully thank Peter Knecht, Anthoula Papageorgiou, and Joachim Reichert for their support with the STM.

■ REFERENCES

(1) Trimpin, S.; Marshall, D. D.; Karki, S.; Madarshahian, S.; Hoang, K.; Meher, A. K.; Pophristic, M.; Richards, A. L.; Lietz, C. B.; Fischer, J. L.; Elia, E. A.; Wang, B.; Pagnotti, V. S.; Lutomski, C. A.; El-Baba, T. J.; Lu, I.-C.; Wager-Miller, J.; Mackie, K.; McEwen, C. N.; Inutan, E. D. *Rapid Commun. Mass Spectrom.* **2020**, *35*, No. e8829.
(2) Gross, J. H. In *Mass Spectrometry A Textbook*, 3rd ed.; Gross, J. H., Ed.; Springer, 2017.
(3) Takats, Z.; Wiseman, J. M.; Gologan, B.; Cooks, R. G. *Science* **2004**, *306*, 471.
(4) Cooks, R. G.; Ouyang, Z.; Takats, Z.; Wiseman, J. M. *Science* **2006**, *311*, 1566.
(5) Monge, M. E.; Harris, G. A.; Dwivedi, P.; Fernandez, F. M. *Chem. Rev.* **2013**, *113*, 2269.
(6) Verbeck, G.; Hoffmann, W.; Walton, B. *Analyst* **2012**, *137*, 4393.
(7) Laskin, J.; Johnson, G. E.; Warneke, J.; Prabhakaran, V. *Angew. Chem.* **2018**, *57*, 16270−16284.
(8) Krumbein, L.; Anggara, K.; Stella, M.; Michnowicz, T.; Ochner, H.; Abb, S.; Rinke, G.; Portz, A.; Dürr, M.; Schlickum, U.; Baldwin, A.; Floris, A.; Kern, K.; Rauschenbach, S. *Phys. Rev. Lett.* **2021**, *126*, No. 056001.
(9) Anggara, K.; Zhu, Y.; Delbianco, M.; Rauschenbach, S.; Abb, S.; Seeberger, P. H.; Kern, K. *J. Am. Chem. Soc.* **2020**, *142*, 21420−21427.
(10) Berggren, K. K.; Bard, A.; Wilbur, J. L.; Gillaspy, J. D.; Helg, A. G.; McClelland, J. J.; Rolston, S. L.; Phillips, W. D.; Prentiss, M.; Whitesides, G. M. *Science* **1995**, *269*, 1255−1257.
(11) Watt, F.; Bettiol, A. A.; Kan, J. A. V.; Teo, E. J.; Breese, M. B. H. *Int. J. Nanosci.* **2005**, *4*, 269−286.
(12) Drost, M.; Tu, F.; Berger, L.; Preischl, C.; Zhou, W.; Gliemann, H.; Wöll, C.; Marbach, H. *ACS Nano* **2018**, *12*, 3825−3835.
(13) Franchetti, V.; Solka, B. H.; Baitinger, W. E.; Amy, J. W.; Cooks, R. G. *Int. J. Mass Spectrom. Ion Phys.* **1977**, *23*, 29−35.
(14) Pradeep, T.; Feng, B.; Ast, T.; Patrick, J. S.; Cooks, R. G.; Pachuta, S. J. *J. Am. Soc. Mass Spectrom.* **1995**, *6*, 187−194.

(15) Miller, S. A.; Luo, H.; Pachuta, S. J.; Cooks, R. G. *Science* **1997**, *275*, 1447−1450.
(16) Luo, H.; Miller, S. A.; Cooks, R. G.; Pachuta, S. J. *Int. J. Mass Spectrom. Ion Processes* **1998**, *174*, 193−217.
(17) Feng, B.; Wunschel, D. S.; Masselon, C. D.; Pasa-Tolic, L.; Smith, R. D. *J. Am. Chem. Soc.* **1999**, *121*, 8961−8962.
(18) Cyriac, J.; Pradeep, T.; Kang, H.; Souda, R.; Cooks, R. G. *Chem. Rev.* **2012**, *112*, 5356−5411.
(19) Laskin, J.; Denisov, E. V.; Shukla, A. K.; Barlow, S. E.; Futrell, J. H. *Anal. Chem.* **2002**, *74*, 3255−3261.
(20) Alvarez, J.; Cooks, R. G.; Barlow, S. E.; Gaspar, D. J.; Futrell, J. H.; Laskin, J. *Anal. Chem.* **2005**, *77*, 3452−3460.
(21) Gologan, B.; Green, J. R.; Alvarez, J.; Laskin, J.; Cooks, R. G. *Phys. Chem. Chem. Phys.* **2005**, *7*, 1490.
(22) Wang, P.; Hadjar, O.; Gassman, P. L.; Laskin, J. *Phys. Chem. Chem. Phys.* **2008**, *10*, 1512−1522.
(23) Johnson, G. E.; Lysonski, M.; Laskin, J. *Anal. Chem.* **2010**, *82*, 5718−5727.
(24) Johnson, G. E.; Laskin, J. *Chem.—Eur. J.* **2010**, *16*, 14433−14438.
(25) Laskin, J. *Int. J. Mass Spectrom.* **2015**, *377*, 188−200.
(26) Johnson, G. E.; Gunaratne, D.; Laskin, J. *Mass Spectrom. Rev.* **2016**, *35*, 439−479.
(27) Jacobs, D. C. *Annu. Rev. Phys. Chem.* **2002**, *53*, 379−407.
(28) Mikhailov, V. A.; Mize, T. H.; Benesch, J. L. P.; Robinson, C. V. *Anal. Chem.* **2014**, *86*, 8321−8328.
(29) Kahle, S.; Deng, Z.; Malinowski, N.; Tonnoir, C.; Forment-Aliaga, A.; Thontasen, N.; Rinke, G.; Le, D.; Turkowski, V.; Rahman, T. S.; Rauschenbach, S.; Ternes, M.; Kern, K. *Nano Lett.* **2012**, *12*, 518−521.
(30) Nagaoka, S.; Matsumoto, T.; Ikemoto, K.; Mitsui, M.; Nakajima, A. *J. Am. Chem. Soc.* **2007**, *129*, 1528−1529.
(31) Peng, W.-P.; Johnson, G. E.; Fortmeyer, I. C.; Wang, P.; Hadjar, O.; Cooks, R. G.; Laskin, J. *Phys. Chem. Chem. Phys.* **2011**, *13*, 267−275.
(32) Hauptmann, N.; Hamann, C.; Tang, H.; Berndt, R. *J. Chem. Phys.* **2013**, *117*, 9734−9738.
(33) Pepi, F.; Ricci, A.; Tata, A.; Favero, G.; Frasconi, M.; Noci, S. D.; Mazzei, F. *Chem. Commun.* **2007**, 3494.
(34) Hauptmann, N.; Scheil, K.; Gopakumar, T. G.; Otte, F. L.; Schütt, C.; Herges, R.; Berndt, R. *J. Am. Chem. Soc.* **2013**, *135*, 8814−8817.
(35) Wijesundara, M. B. J.; Fuoco, E.; Hanley, L. *Langmuir* **2001**, *17*, 5721−5726.
(36) Shen, J.; Yim, Y. H.; Feng, B.; Grill, V.; Evans, C.; Cooks, R. G. *Int. J. Mass Spectrom.* **1999**, *182−183*, 423−435.
(37) Qin, X.; Tzvetkov, T.; Jacobs, D. C. *J. Phys. Chem. A* **2006**, *110*, 1408−1415.
(38) Klipp, B.; Grass, M.; Müller, J.; Stolcic, D.; Lutz, U.; Ganteför, G.; Schlenker, T.; Boneberg, J.; Leiderer, P. *Appl. Phys. A: Mater. Sci. Process.* **2001**, *73*, 547−554.
(39) Palmer, R. E.; Pratontep, S.; Boyen, H.-G. *Nat. Mater.* **2003**, *2*, 443−448.
(40) Heiz, U.; Bullock, E. L. *J. Mater. Chem.* **2004**, *14*, 564.
(41) Rauschenbach, S.; Stadler, F. L.; Lunedei, E.; Malinowski, N.; Koltsov, S.; Costantini, G.; Kern, K. *Small* **2006**, *2*, 540−547.
(42) Vajda, S.; White, M. G. *ACS Catal.* **2015**, *5*, 7152−7176.
(43) Laskin, J.; Johnson, G. E.; Prabhakaran, V. *J. Phys. Chem. C* **2016**, *120*, 23305−23322.
(44) Vats, N.; Wang, Y.; Sen, S.; Szilagyi, S.; Ochner, H.; Abb, S.; Burghard, M.; Sigle, W.; Kern, K.; Aken van, P. A.; Rauschenbach, S. *ACS Nano* **2020**, *14*, 4626−4635.
(45) Kaden, W. E.; Wu, T.; Kunkel, W. A.; Anderson, S. L. *Science* **2009**, *326*, 826−829.
(46) Tyo, E. C.; Vajda, S. *Nat. Nanotechnol.* **2015**, *10*, 577−588.
(47) Ha, M.-A.; Baxter, E. T.; Cass, A. C.; Anderson, S. L.; Alexandrova, A. N. *J. Am. Chem. Soc.* **2017**, *139*, 11568−11575.
(48) Xu, J.; Murphy, S.; Xiong, D.; Cai, R.; Wei, X.-K.; Heggen, M.; Barborini, E.; Vinati, S.; Dunin-Borkowski, R. E.; Palmer, R. E.; Liu, L. *ACS Appl. Energy Mater.* **2018**, *1*, 3013−3018.
(49) Böttcher, A.; Weis, P.; Jester, S.-S.; Loeffler, D.; Bihlmeier, A.; Klopper, W.; Kappes, M. M. *Phys. Chem. Chem. Phys.* **2005**, *7*, 2816.
(50) Dubey, G.; Urcuyo, R.; Abb, S.; Rinke, G.; Burghard, M.; Rauschenbach, S.; Kern, K. *J. Am. Chem. Soc.* **2014**, *136*, 13482−13485.
(51) Pepi, F.; Tata, A.; Garzoli, S.; Giacomello, P.; Ragno, R.; Patsilinakos, A.; Fusco, M. D.; D'Annibale, A.; Cannistraro, S.; Baldacchini, C.; Favero, G.; Frasconi, M.; Mazzei, F. *J. Phys. Chem. C* **2011**, *115*, 4863−4871.
(52) Ulrich Stützel, E.; Dufaux, T.; Sagar, A.; Rauschenbach, S.; Balasubramanian, K.; Burghard, M.; Kern, K. *Appl. Phys. Lett.* **2013**, *102*, No. 043106.
(53) Rinke, G.; Rauschenbach, S.; Schrettl, S.; Hoheisel, T. N.; Blohm, J.; Gutzler, R.; Rosei, F.; Frauenrath, H.; Kern, K. *Int. J. Mass Spectrom.* **2015**, *377*, 228−234.
(54) Fodor, S.; Read, J.; Pirrung, M.; Stryer, L.; Lu, A.; Solas, D. *Science* **1991**, *251*, 767−773.
(55) Zhu, H.; Bilgin, M.; Bangham, R.; Hall, D.; Casamayor, A.; Bertone, P.; Lan, N.; Jansen, R.; Bidlingmaier, S.; Houfek, T.; Mitchell, T.; Miller, P.; Dean, R. A.; Gerstein, M.; Snyder, M. *Science* **2001**, *293*, 2101−2105.
(56) Reineke, U.; Volkmer-Engert, R.; Schneider-Mergener, J. *Curr. Opin. Biotechnol.* **2001**, *12*, 59−64.
(57) Reimer, U.; Reineke, U.; Schneider-Mergener, J. *Curr. Opin. Biotechnol.* **2002**, *13*, 315−320.
(58) Wong, L. S.; Khan, F.; Micklefield, J. *Chem. Rev.* **2009**, *109*, 4025−4053.
(59) Ouyang, Z.; Takats, Z.; Blake, T. A.; Gologan, B.; Guymon, A. J.; Wiseman, J. M.; Oliver, J. C.; Davisson, V. J.; Cooks, R. G. *Science* **2003**, *301*, 1351−1354.
(60) Blake, T. A.; Ouyang, Z.; Wiseman, J. M.; Takats, Z.; Guymon, A. J.; Kothari, S.; Cooks, R. G. *Anal. Chem.* **2004**, *76*, 6293−6305.
(61) Wang, P.; Laskin, J. *Angew. Chem.* **2008**, *47*, 6678−6680.
(62) Laskin, J.; Hu, Q. *J. Am. Soc. Mass Spectrom.* **2017**, *28*, 1304−1312.
(63) Hamann, C.; Woltmann, R.; Hong, I.-P.; Hauptmann, N.; Karan, S.; Berndt, R. *Rev. Sci. Instrum.* **2011**, *82*, No. 033903.
(64) Hu, Q.; Laskin, J. *J. Phys. Chem. B* **2016**, *120*, 4927−4936.
(65) Abb, S.; Tarrat, N.; Cortes, J.; Andriyevsky, B.; Harnau, L.; Schön, J. C.; Rauschenbach, S.; Kern, K. *Angew. Chem.* **2019**, *58*, 8336−8340.
(66) Wu, X.; Delbianco, M.; Anggara, K.; Michnowicz, T.; Pardo-Vargas, A.; Bharate, P.; Sen, S.; Pristl, M.; Rauschenbach, S.; Schlickum, U.; Abb, S.; Seeberger, P. H.; Kern, K. *Nature* **2020**, *582*, 375−378.
(67) Anggara, K.; Zhu, Y.; Fittolani, G.; Yu, Y.; Tyrikos-Ergas, T.; Delbianco, M.; Rauschenbach, S.; Abb, S.; Seeberger, P. H.; Kern, K. *Proc. Natl. Acad. Sci. U.S.A.* **2021**, *118*, No. e2102168118.
(68) Paul, W.; Steinwedel, H. *Z. Naturforsch. A* **1953**, *8*, 448−450.
(69) Paul, W.; Raether, M. *Z. Phys.* **1955**, *140*, 262−273.
(70) Paul, W.; Reinhard, H. P.; von Zahn, U. *Z. Phys.* **1958**, *152*, 143−182.
(71) Von Zahn, U. *Rev. Sci. Instrum.* **1963**, *34*, 1−4.
(72) Gerlich, D. *J. Chem. Soc., Faraday Trans.* **1993**, *89*, 2199−2208.
(73) Dzhonson, A.; Gerlich, D.; Bieske, E. J.; Maier, J. P. *J. Mol. Struct.* **2006**, *795*, 93−97.
(74) Otto, R.; Hlavenka, P.; Trippel, S.; Mikosch, J.; Singer, K.; Weidemüller, M.; Wester, R. *J. Phys. B: At., Mol. Opt. Phys.* **2009**, *42*, No. 154007.
(75) Lorenz, U. J.; Rizzo, T. R. *Anal. Chem.* **2011**, *83*, 7895−7901.
(76) Asvany, O.; Bielau, F.; Moratschke, D.; Krause, J.; Schlemmer, S. *Rev. Sci. Instrum.* **2010**, *81*, No. 076102.
(77) Hayashi, T.; Sakudo, N. *Rev. Sci. Instrum.* **1968**, *39*, 958−961.
(78) Dawson, P. H.; Whetten, N. R. *J. Vac. Sci. Technol.* **1970**, *7*, 440−441.
(79) Denison, D. R. *J. Vac. Sci. Technol.* **1971**, *8*, 266−269.
(80) Lee-Whiting, G. E.; Yamazaki, L. *Nucl. Instrum. Methods* **1971**, *94*, 319−332.
(81) Pearce, C. G.; Halsall, D. *Int. J. Mass Spectrom. Ion Phys.* **1978**, *27*, 31−41.
(82) Beaty, E. C. *J. Appl. Phys.* **1987**, *61*, 2118−2122.

https://doi.org/10.1021/acs.analchem.1c04495
Anal. Chem. 2022, 94, 7767−7778

(83) Hunter, K. L.; Mcintosh, B. J. *Int. J. Mass Spectrom. Ion Processes* **1989**, *87*, 157−164.
(84) Gerlich, D. Inhomogeneous Rf Fields: A Versatile Tool for the Study of Processes with Slow Ions. *Advances in Chemical Physics*; John Wiley & Sons, Inc., 1992; Vol. *82*, p 671.
(85) Schulte, J.; Shevchenko, P. V.; Radchik, A. V. *Rev. Sci. Instrum.* **1999**, *70*, 3566−3571.
(86) Gibson, J. R.; Taylor, S. *Rapid Commun. Mass Spectrom.* **2000**, *14*, 1669−1673.
(87) Gibson, J. R.; Taylor, S. *Rapid Commun. Mass Spectrom.* **2001**, *15*, 1960−1964.
(88) Gibson, J. R.; Taylor, S. *Rapid Commun. Mass Spectrom.* **2003**, *17*, 1051−1055.
(89) Ding, C.; Konenkov, N. V.; Douglas, D. J. *Rapid Commun. Mass Spectrom.* **2003**, *17*, 2495−2502.
(90) Konenkov, N.; Londry, F.; Ding, C.; Douglas, D. J. *J. Am. Soc. Mass Spectrom.* **2006**, *17*, 1063−1073.
(91) Salazar, G. A.; Masujima, T. *J. Am. Soc. Mass Spectrom.* **2007**, *18*, 413−421.
(92) Moradian, A.; Douglas, D. J. *J. Am. Soc. Mass Spectrom.* **2008**, *19*, 270−280.
(93) Douglas, D. J. *Mass Spectrom. Rev.* **2009**, *28*, 937−960.
(94) Xiao, Z.; Zhao, X.; Douglas, D. J. *Rapid Commun. Mass Spectrom.* **2010**, *24*, 1985−1992.
(95) Zhou, X.; Xiong, C.; Xu, G.; Liu, H.; Tang, Y.; Zhu, Z.; Chen, R.; Qiao, H.; Tseng, Y.-H.; Peng, W.-P.; Nie, Z.; Chen, Y. *J. Am. Soc. Mass Spectrom.* **2011**, *22*, 386−398.
(96) Douglas, D. J.; Konenkov, N. V. *Rapid Commun. Mass Spectrom.* **2014**, *28*, 2252−2258.
(97) Shaffer, S. A.; Tang, K.; Anderson, G. A.; Prior, D. C.; Udseth, H. R.; Smith, R. D.; Novel Ion, A. *Rapid Commun. Mass Spectrom.* **1997**, *11*, 1813−1817.
(98) Shaffer, S. A.; Prior, D. C.; Anderson, G. A.; Udseth, H. R.; Smith, R. D. *Anal. Chem.* **1998**, *70*, 4111−4119.
(99) Shaffer, S. A.; Tolmachev, A.; Prior, D. C.; Anderson, G. A.; Udseth, H. R.; Smith, R. D. *Anal. Chem.* **1999**, *71*, 2957−2964.
(100) Tolmachev, A. V.; Udseth, H. R.; Smith, R. D. *Anal. Chem.* **2000**, *72*, 970−978.
(101) Kim, T.; Tang, K.; Udseth, H. R.; Smith, R. D. *Anal. Chem.* **2001**, *73*, 4162−4170.
(102) Tang, K.; Shvartsburg, A. A.; Lee, H.-N.; Prior, D. C.; Buschbach, M. A.; Li, F.; Tolmachev, A. V.; Anderson, G. A.; Smith, R. D. *Anal. Chem.* **2005**, *77*, 3330−3339.
(103) Page, J. S.; Tolmachev, A. V.; Tang, K.; Smith, R. D. *J. Mass Spectrom.* **2005**, *40*, 1215−1222.
(104) Bahr, R.; Gerlich, D.; Teloy, E. *Verh. Deutsch. Phys. Ges.* **1969**, *4*, 343.
(105) Teloy, E.; Gerlich, D. *Chem. Phys.* **1974**, *4*, 417−427.
(106) Gerlich, D.; Kaefer, G. *Astrophys. J.* **1989**, *347*, 849.
(107) Guan, S.; Marshall, A. G. *J. Am. Soc. Mass Spectrom.* **1996**, *7*, 101−106.
(108) Swarbrick, J. C.; Taylor, J. B.; O'Shea, J. N. *Appl. Surf. Sci.* **2006**, *252*, 5622−5626.
(109) Satterley, C. J.; Perdigao, L. M. A.; Saywell, A.; Magnano, G.; Rienzo, A.; Mayor, L. C.; Dhanak, V. R.; Beton, P. H.; O'Shea, J. N. *Nanotechnology* **2007**, *18*, No. 455304.
(110) Mayor, L. C.; Taylor, J. B.; Magnano, G.; Rienzo, A.; Satterley, C. J.; O'Shea, J. N.; Schnadt, J. *J. Chem. Phys.* **2008**, *129*, No. 114701.
(111) Tanaka, H.; Kawai, T. *J. Vac. Sci. Technol., B: Microelectron. Nanometer Struct.—Process., Meas., Phenom.* **1997**, *15*, 602.
(112) Yamada, T.; Shinohara, H.; Maofa, G.; Mashiko, S.; Kimura, K. *Chem. Phys. Lett.* **2003**, *370*, 132−138.
(113) Grill, L.; Stass, I.; Rieder, K.-H.; Moresco, F. *Surf. Sci.* **2006**, *600*, L143−L147.
(114) Yamada, T.; Shinohara, H.; Kamikado, T.; Mashiko, S. *Jpn. J. Appl. Phys.* **2008**, *47*, 1408−1411.
(115) Kitching, K. J.; Lee, H.-N.; Elam, W. T.; Johnston, E. E.; MacGregor, H.; Miller, R. J.; Turecek, F.; Ratner, B. D. *Rev. Sci. Instrum.* **2003**, *74*, 4832−4839.
(116) Volný, M.; Elam, W. T.; Branca, A.; Ratner, B. D.; Turecek, F. *Anal. Chem.* **2005**, *77*, 4890−4896.
(117) Volný, M.; Elam, W. T.; Ratner, B. D.; Turecek, F. *Anal. Chem.* **2005**, *77*, 4846−4853.
(118) Clemmons, J. H.; Herrero, F. A. *Rev. Sci. Instrum.* **1998**, *69*, 2285−2291.
(119) Nojima, M.; Anai, Y.; Hotta, M.; Kurumi, S.; Suzuki, K.; Adachi, T.; Kusanagi, T.; Moritani, K. *J. Vac. Sci. Technol., B: Nanotechnol. Microelectron.: Mater., Process., Meas., Phenom.* **2016**, *34*, No. 03H132.
(120) Su, P.; Espenship, M. F.; Laskin, J. *J. Am. Soc. Mass Spectrom.* **2020**, *31*, 1875−1884.
(121) Su, P.; Hu, H.; Unsihuay, D.; Zhang, D.; Dainese, T.; Diaz, R. E.; Lee, J.; Gunaratne, D. K.; Wang, H.; Maran, F.; Mei, J.; Laskin, J. *Angew. Chem.* **2020**, *132*, 7785−7790.
(122) Foret, F.; Zhou, H.; Gangl, E.; Karger, B. L. *Electrophoresis* **2000**, *21*, 1363−1371.
(123) Page, J. S.; Tang, K.; Kelly, R. T.; Smith, R. D. *Anal. Chem.* **2008**, *80*, 1800−1805.
(124) Gamero-Castaño, M. *J. Fluid Mech.* **2008**, *604*, 339−368.
(125) Marginean, I.; Page, J. S.; Tolmachev, A. V.; Tang, K.; Smith, R. D. *Anal. Chem.* **2010**, *82*, 9344−9349.
(126) Cox, J. T.; Marginean, I.; Kelly, R. T.; Smith, R. D.; Tang, K. *J. Am. Soc. Mass Spectrom.* **2014**, *25*, 2028−2037.
(127) Debatin, M.; Kröner, M.; Mikosch, J.; Trippel, S.; Morrison, N.; Reetz-Lamour, M.; Woias, P.; Wester, R.; Weidemüller, M. *Phys. Rev. A* **2008**, *77*, No. 033422.
(128) Tolmachev, A. V.; Webb, I. K.; Ibrahim, Y. M.; Garimella, S. V. B.; Zhang, X.; Anderson, G. A.; Smith, R. D. *Anal. Chem.* **2014**, *86*, 9162−9168.
(129) Attah, I. K.; Garimella, S. V. B.; Webb, I. K.; Nagy, G.; Norheim, R. V.; Schimelfenig, C. E.; Ibrahim, Y. M.; Smith, R. D. *J. Am. Soc. Mass Spectrom.* **2019**, *30*, 967−976.
(130) Rulison, A. J.; Flagan, R. C. *Rev. Sci. Instrum.* **1993**, *64*, 683−686.
(131) Sen, A. K.; Darabi, J.; Knapp, D. R. *Microfluid. Nanofluid.* **2007**, *3*, 283−298.
(132) Page, J. S.; Kelly, R. T.; Tang, K.; Smith, R. D. *J. Am. Soc. Mass Spectrom.* **2007**, *18*, 1582−1590.
(133) Mayer, P. S.; Turecek, F.; Lee, H.-N.; Scheidemann, A. A.; Olney, T. N.; Schumacher, F.; Strop, P.; Smrcina, M.; Patek, M.; Schirlin, D. *Anal. Chem.* **2005**, *77*, 4378−4384.
(134) Yang, X.; Mayer, P. S.; Turecek, F. *J. Mass Spectrom.* **2006**, *41*, 256−262.
(135) Pauly, M.; Sroka, M.; Reiss, J.; Rinke, G.; Albarghash, A.; Vogelgesang, R.; Hahne, H.; Kuster, B.; Sesterhenn, J.; Kern, K.; Rauschenbach, S. *Analyst* **2014**, *139*, 1856.
(136) Bernier, L.; Pinfold, H.; Pauly, M.; Rauschenbach, S.; Reiss, J. *J. Am. Soc. Mass Spectrom.* **2018**, *29*, 761−773.
(137) Bernier, L.; Taesch, M.; Rauschenbach, S.; Reiss, J. *Int. J. Mass Spectrom.* **2019**, *447*, No. 116239.
(138) Tang, K.; Tolmachev, A. V.; Nikolaev, E.; Zhang, R.; Belov, M. E.; Udseth, H. R.; Smith, R. D. *Anal. Chem.* **2002**, *74*, 5431−5437.
(139) Deng, L.; Chen, X.; Li, W.; Wang, Z.; Wong, Y. E.; Chan, T.-W. D. *Anal. Chem.* **2015**, *87*, 8073−8077.
(140) Goldby, I. M.; Issendorff von, B.; Kuipers, L.; Palmer, R. E. *Rev. Sci. Instrum.* **1997**, *68*, 3327−3334.
(141) Hamann, C. An Electrospray Ion Source for Ultra-High Vacuum Deposition of Organic Molecules. Ph.D. Thesis, Christian-Albrechts-Universität zu Kiel, 2011.
(142) Heiz, U.; Vanolli, F.; Trento, L.; Schneider, W.-D. *Rev. Sci. Instrum.* **1997**, *68*, 1986−1994.
(143) Hadjar, O.; Wang, P.; Futrell, J. H.; Dessiaterik, Y.; Zhu, Z.; Cowin, J. P.; Iedema, M. J.; Laskin, J. *Anal. Chem.* **2007**, *79*, 6566−6574.
(144) Hadjar, O.; Futrell, J. H.; Laskin, J. *J. Phys. Chem. C* **2007**, *111*, 18220−18225.
(145) Laskin, J.; Wang, P.; Hadjar, O. *Phys. Chem. Chem. Phys.* **2008**, *10*, 1079−1090.

https://doi.org/10.1021/acs.analchem.1c04495
Anal. Chem. 2022, 94, 7767−7778

(146) Kern, B.; Greisch, J.-F.; Strelnikov, D.; Weis, P.; Boettcher, A.; Ruben, M.; Schaefer, B.; Schooss, D.; Kappes, M. M. *Anal. Chem.* **2015**, *87*, 11901−11906.
(147) Gunaratne, K. D. D.; Prabhakaran, V.; Ibrahim, Y. M.; Norheim, R. V.; Johnson, G. E.; Laskin, J. *Analyst* **2015**, *140*, 2957−2963.
(148) Peng, W.-P.; Goodwin, M. P.; Nie, Z.; Volny, M.; Ouyang, Z.; Cooks, R. G. *Anal. Chem.* **2008**, *80*, 6640−6649.
(149) Nie, Z.; Li, G.; Goodwin, M. P.; Gao, L.; Cyriac, J.; Cooks, R. G. *J. Am. Soc. Mass Spectrom.* **2009**, *20*, 949−956.
(150) Su, P.; Hu, H.; Warneke, J.; Belov, M. E.; Anderson, G. A.; Laskin, J. *Anal. Chem.* **2019**, *91*, 5904−5912.
(151) Kurulugama, R. T.; Belov, M. E. Orthogonal Ion Injection Apparatus and Process. US8,698,075B2, 2014.
(152) Chen, T.-C.; Fillmore, T. L.; Prost, S. A.; Moore, R. J.; Ibrahim, Y. M.; Smith, R. D. *Anal. Chem.* **2015**, *87*, 7326−7331.
(153) Su, P.; Chen, X.; Smith, A. J.; Espenship, M. F.; Oviedo, H. Y. S.; Wilson, S. M.; Gholipour-Ranjbar, H.; Larriba-Andaluz, C.; Laskin, J. *Anal. Chem.* **2021**, *93*, 11576−11584.
(154) Dawson, P. H. *Mass Spectrom. Rev.* **1986**, *5*, 1−37.
(155) Marshall, A. G.; Schweikhard, L. *Int. J. Mass Spectrom. Ion Processes* **1992**, *118*−*119*, 37−70.
(156) Hu, Q.; Noll, R. J.; Li, H.; Makarov, A.; Hardman, M.; Cooks, R. G. *J. Mass Spectrom.* **2005**, *40*, 430−443.
(157) Perry, R. H.; Cooks, R. G.; Noll, R. J. *Mass Spectrom. Rev.* **2008**, *27*, 661−699.
(158) Michalski, A.; Damoc, E.; Lange, O.; Denisov, E.; Nolting, D.; Müller, M.; Viner, R.; Schwartz, J.; Remes, P.; Belford, M.; Dunyach, J.-J.; Cox, J.; Horning, S.; Mann, M.; Makarov, A. *Mol. Cell. Proteomics* **2011**, *11*, No. O111.013698.
(159) Ding, L.; Rusinov, A. *Anal. Chem.* **2019**, *91*, 7595−7602.
(160) Rusinov, A.; Ding, L.; Smirnov, S.; Knight, P.; Andrzejewski, R.; Waki, H. *J. Am. Soc. Mass Spectrom.* **2021**, *32*, 1145−1154.
(161) Pratontep, S.; Carroll, S. J.; Xirouchaki, C.; Streun, M.; Palmer, R. E. *Rev. Sci. Instrum.* **2005**, *76*, No. 045103.
(162) Richards, J. A.; Huey, R. M.; Hiller, J. *Int. J. Mass Spectrom. Ion Phys.* **1973**, *12*, 317−339.
(163) Sheretov, E. P.; Gurov, V. S.; Safonov, M. P.; Philippov, I. W. *Int. J. Mass Spectrom.* **1999**, *189*, 9−17.
(164) Shinholt, D. L.; Anthony, S. N.; Alexander, A. W.; Draper, B. E.; Jarrold, M. F. *Rev. Sci. Instrum.* **2014**, *85*, No. 113109.
(165) Gotlib, Z. P.; Brabeck, G. F.; Reilly, P. T. A. *Anal. Chem.* **2017**, *89*, 4287−4293.
(166) Hoffman, N. M.; Gotlib, Z. P.; Opacic, B.; Clowers, B. H.; Reilly, P. T. A. *Rev. Sci. Instrum.* **2018**, *89*, No. 084101.
(167) Opačić, B.; Huntley, A. P.; Clowers, B. H.; Reilly, P. T. A. *J. Mass Spectrom.* **2018**, *53*, 1155−1168.
(168) Huntley, A. P.; Reilly, P. T. A. *J. Mass Spectrom.* **2021**, *56*, No. e4699.
(169) Kelly, R. T.; Tolmachev, A. V.; Page, J. S.; Tang, K.; Smith, R. D. *Mass Spectrom. Rev.* **2009**, *30*, 294−312.
(170) Ibrahim, Y. M.; Baker, E. S.; Danielson, W. F.; Norheim, R. V.; Prior, D. C.; Anderson, G. A.; Belov, M. E.; Smith, R. D. *Int. J. Mass Spectrom.* **2015**, *377*, 655−662.
(171) Ford, M. J.; Kertesz, V.; Berkel, G. J. V. *J. Mass Spectrom.* **2005**, *40*, 866−875.
(172) Yamada, T.; Shinohara, H.; Mashiko, S. *Thin Solid Films* **2006**, *499*, 44−48.
(173) Volný, M.; Sengupta, A.; Wilson, C. B.; Swanson, B. D.; Davis, E. J.; Turecek, F. *Anal. Chem.* **2007**, *79*, 4543−4551.
(174) Wortmann, A.; Kistler-Momotova, A.; Zenobi, R.; Heine, M. C.; Wilhelm, O.; Pratsinis, S. E. *J. Am. Soc. Mass Spectrom.* **2007**, *18*, 385−393.
(175) Rauschenbach, S.; Vogelgesang, R.; Malinowski, N.; Gerlach, J. W.; Benyoucef, M.; Costantini, G.; Deng, Z.; Thontasen, N.; Kern, K. *ACS Nano* **2009**, *3*, 2901−2910.
(176) Law, W. S.; Wang, R.; Hu, B.; Berchtold, C.; Meier, L.; Chen, H.; Zenobi, R. *Anal. Chem.* **2010**, *82*, 4494−4500.
(177) Cyriac, J.; Wleklinski, M.; Li, G.; Gao, L.; Cooks, R. G. *Analyst* **2012**, *137*, 1363.
(178) Clemen, M.; Gernert, C.; Peters, J.; Grotemeyer, J. *Eur. J. Mass Spectrom.* **2013**, *19*, 135−139.
(179) Bluck, L.; Volmer, D. A. *Spectroscopy* **2009**, *23*, 36.
(180) Bluck, L.; Volmer, D. A. *Spectroscopy* **2009**, *23*, 50.
(181) Geiger, R. J.; Melnyk, M. C.; Busch, K. L.; Bartlett, M. G. *Int. J. Mass Spectrom.* **1999**, *182*−*183*, 415−422.
(182) Benesch, J. L. P.; Ruotolo, B. T.; Simmons, D. A.; Barrera, N. P.; Morgner, N.; Wang, L.; Saibil, H. R.; Robinson, C. V. *J. Struct. Biol.* **2010**, *172*, 161−168.
(183) *PubChem Compound Summary for CID 118984375: Insulin Human—Compound Summary*; National Center for Biotechnology Information, 2021. https://pubchem.ncbi.nlm.nih.gov/compound/118984375.
(184) P01308: UniProtKB Human Insulin. *Nucleic Acids Res.* 2021, *49*, D1. https://www.uniprot.org/uniprot/P01308.
(185) Derewenda, U.; Derewenda, Z.; Dodson, G. G.; Hubbard, R. E.; Korber, F. *Br. Med. Bull.* **1989**, *45*, 4−18.
(186) Pekar, A. H.; Frank, B. H. *Biochemistry* **1972**, *11*, 4013−4016.
(187) Nettleton, E. J.; Tito, P.; Sunde, M.; Bouchard, M.; Dobson, C. M.; Robinson, C. V. *Biophys. J.* **2000**, *79*, 1053−1065.
(188) Attri, A. K.; Fernandez, C.; Minton, A. P. *Biophys. Chem.* **2010**, *148*, 28−33.
(189) Lin, M.; Larive, C. K. *Anal. Biochem.* **1995**, *229*, 214−220.
(190) Kadima, W.; Roy, M.; Lee, R. W.-K.; Kaarsholmj, N. C.; Dunn, M. F. *J. Biol. Chem.* **1992**, *267*, 8963−8970.
(191) Dunn, M. F. *BioMetals* **2005**, *18*, 295−303.
(192) Attri, A. K.; Fernandez, C.; Minton, A. P. *Biophys. Chem.* **2010**, *148*, 23−27.
(193) Kadima, W.; Ogendal, L.; Bauer, R.; Kaarsholm, N.; Brodersen, K.; Hansen, J. F.; Porting, P. *Biopolymers* **1993**, *33*, 1643−1657.
(194) Rahuel-Clermont, S.; French, C. A.; Kaarsholm, N. C.; Dunn, M. F. *Biochemistry* **1997**, *36*, 5837−5845.
(195) Kumar, A.; Venkatesu, P. *RSC Adv.* **2013**, *3*, 362−367.
(196) Kaltashov, I. A.; Mohimen, A. *Anal. Chem.* **2005**, *77*, 5370.
(197) Schmidt, A.; Karas, M.; Dülcks, T. *J. Am. Soc. Mass Spectrom.* **2003**, *14*, 492−500.
(198) Rayleigh, L. *London, Edinburgh Dublin Philos. Mag. J. Sci.* **1882**, *14*, 184−186.
(199) Bonvin, G.; Rudaz, S.; Schappler, J. *Anal. Chim. Acta* **2014**, *813*, 97−105.
(200) Susa, A. C.; Xia, Z.; Williams, E. R. *Anal. Chem.* **2017**, *89*, 3116−3122.
(201) Hu, J.; Guan, Q.-Y.; Wang, J.; Jiang, X.-X.; Wu, Z.-Q.; Xia, X.-H.; Xu, J.-J.; Chen, H.-Y. *Anal. Chem.* **2017**, *89*, 1838−1845.
(202) Fabris, D.; Fenselau, C. *Anal. Chem.* **1999**, *71*, 384−387.
(203) Rauschenbach, S. Sodium and Potassium Ions Are Typical Satellites in MS. Private communication, 2020.
(204) Raja, U. K. B.; Injeti, S.; Culver, T.; McCabe, J. W.; Angel, L. A. *Eur. J. Mass Spectrom.* **2015**, *21*, 759−774.
(205) Stoiber, K. A. Investigating Molecules at Surfaces—From Preparative Mass Spectrometry of Large Biomolecules to Complex Desorption Kinetics. Ph.D. Thesis, Technische Uni München, 2021.
(206) Otsuki, J. *Coord. Chem. Rev.* **2010**, *254*, 2311−2341.
(207) Auwärter, W.; Ecija, D.; Klappenberger, F.; Barth, J. V. *Nat. Chem.* **2015**, *7*, 105−120.
(208) Zhao, M.; Wang, Y.; Ma, Q.; Huang, Y.; Zhang, X.; Ping, J.; Zhang, Z.; Lu, Q.; Yu, Y.; Xu, H.; Zhao, Y.; Zhang, H. *Adv. Mater.* **2015**, *27*, 7372−7378.
(209) Zhao, M.; Huang, Y.; Peng, Y.; Huang, Z.; Ma, Q.; Zhang, H. *Chem. Soc. Rev.* **2018**, *47*, 6267−6295.
(210) Baig, N.; Kammakakam, I.; Falath, W. *Mater. Adv.* **2021**, *2*, 1821−1871.
(211) Nicholls, D.; McKinzie, W. P.; Oncel, N. *J. Phys. Chem. C* **2010**, *114*, 14983−14985.
(212) Jöhr, R.; Hinaut, A.; Pawlak, R.; Sadeghi, A.; Saha, S.; Goedecker, S.; Such, B.; Szymonski, M.; Meyer, E.; Glatzel, T. *J. Chem. Phys.* **2015**, *143*, No. 094202.

https://doi.org/10.1021/acs.analchem.1c04495
Anal. Chem. 2022, 94, 7767−7778

(213) Freund, S.; Hinaut, A.; Marinakis, N.; Constable, E. C.; Meyer, E.; Housecroft, C. E.; Glatzel, T. *Beilstein J. Nanotechnol.* **2019**, *10*, 874−881.
(214) Hinaut, A.; Pawlak, R.; Meyer, E.; Glatzel, T. *Beilstein J. Nanotechnol.* **2015**, *6*, 1927−1934.
(215) Günther, C.; Karl, N.; Pflaum, J.; Strohmaier, R.; Gompf, B.; Eisenmenger, W.; Müller, M.; Müllen, K. *Langmuir* **2005**, *21*, 656−665.
(216) Davie, E.; Morris, J. H.; Smith, W. E. *Org. Mass Spectrom.* **1974**, *9*, 763−773.
(217) Knecht, P. Cu-TCPP Disintegrates upon OMBE Deposition, CO_2 Peak in MS. Private communication, 2019.
(218) Deng, Z.; Thontasen, N.; Malinowski, N.; Rinke, G.; Harnau, L.; Rauschenbach, S.; Kern, K. *Nano Lett.* **2012**, *12*, 2452.
(219) Vats, N.; Rauschenbach, S.; Sigle, W.; Sen, S.; Abb, S.; Portz, A.; Dürr, M.; Burghard, M.; van Aken, P. A.; Kern, K. *Nanoscale* **2018**, *10*, 4952−4961.
(220) Rajabi, K.; Ashcroft, A. E.; Radford, S. E. *Methods* **2015**, *89*, 13−21.
(221) Fremerey, J. K. *Vacuum* **1999**, *53*, 197−201.
(222) Yanisch-Perron, C.; Vieira, J.; Messing, J. *Gene* **1985**, *33*, 103−119.
(223) Nordheim, A.; Knippers, R.; Dröge, P.; Meister, G.; Schiebel, E.; Vingron, M.; Walter, J. In *Molekulare Genetik*; Nordheim, A.; Knippers, R., Eds.; Thieme Verlag KG, 2018.
(224) Cheng, X.; Camp, D. G.; Wu, Q.; Bakhtiar, R.; Springer, D. L.; Morris, B. J.; Bruce, J. E.; Anderson, G. A.; Edmonds, C. G.; Smith, R. D. *Nucleic Acids Res.* **1996**, *24*, 2183−2189.
(225) Schultz, J. C.; Hack, C. A.; Benner, W. H. *J. Am. Soc. Mass Spectrom.* **1998**, *9*, 305−313.
(226) Fuerstenau, S. D.; Benner, W. H. *Rapid Commun. Mass Spectrom.* **1995**, *9*, 1528−1538.
(227) Konermann, L.; Ahadi, E.; Rodriguez, A. D.; Vahidi, S. *Anal. Chem.* **2013**, *85*, 2−9.
(228) Pang, D.; Thierry, A. R.; Dritschilo, A. *Front. Mol. Biosci.* **2015**, *2*, No. 1.
(229) Rauschenbach, S. Accurate Ringshape of Circulare DNA May Be Caused by Electrostatic Repulsion. Private communication, 2020.
(230) Kruve, A.; Rebane, R.; Kipper, K.; Oldekop, M.-L.; Evard, H.; Herodes, K.; Ravio, P.; Leito, I. *Anal. Chim. Acta* **2015**, *870*, 8−28.
(231) Wilm, M.; Mann, M. *Anal. Chem.* **1996**, *68*, 1−8.
(232) El-Faramawy, A.; Siu, K. W. M.; Thomson, B. A. *J. Am. Soc. Mass Spectrom.* **2005**, *16*, 1702−1707.
(233) Volný, M.; Turecek, F. *J. Mass Spectrom.* **2006**, *41*, 124−126.
(234) Cox, J. T.; Marginean, I.; Smith, R. D.; Tang, K. *J. Am. Soc. Mass Spectrom.* **2015**, *26*, 55−62.
(235) Alvarez, J.; Futrell, J. H.; Laskin, J. *J. Phys. Chem. A* **2006**, *110*, 1678−1687.
(236) Gunaratne, K. D. D.; Prabhakaran, V.; Ibrahim, Y. M.; Norheim, R. V.; Johnson, G. E.; Laskin, J. *Analyst* **2015**, *140*, 2957−2963.
(237) Rauschenbach, S.; Rinke, G.; Gutzler, R.; Abb, S.; Albarghash, A.; Le, D.; Rahman, T. S.; Dürr, M.; Harnau, L.; Kern, K. *ACS Nano* **2017**, *11*, 2420−2427.
(238) Wu, X.; Delbianco, M.; Anggara, K.; Michnowicz, T.; Pardo-Vargas, A.; Bharate, P.; Sen, S.; Pristl, M.; Rauschenbach, S.; Schlickum, U.; Abb, S.; Seeberger, P. H.; Kern, K. *Nature* **2020**, *582*, 375−378.
(239) Samayoa-Oviedo, H. Y.; Behrend, K.-A.; Kawa, S.; Knorke, H.; Su, P.; Belov, M. E.; Anderson, G.; Warneke, J.; Laskin, J. *Anal. Chem.* **2021**, *93*, 14489−14496.
(240) Ran, W.; Walz, A.; Stoiber, K.; Knecht, P.; Xu, H.; Papageorgiou, A. C.; Huettig, A.; Cortizo-Lacalle, D.; Mora-Fuentes, J. P.; Mateo-Alonso, A.; Schlichting, H.; Reichert, J.; Barth, J. V. *Angew. Chem., Int. Ed.* **2021**, No. e202111816.

https://doi.org/10.1021/acs.analchem.1c04495
Anal. Chem. 2022, 94, 7767−7778